# Chemical Science

Accepted Manuscript


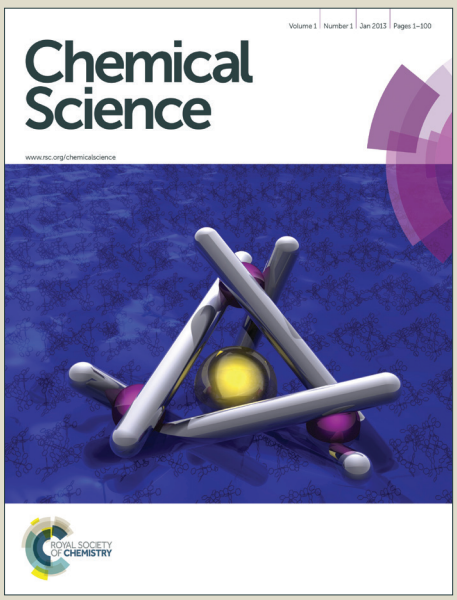





ROYAL SOCIETY OF CHEMISTRY

www.rsc.org/chemicalscience

Journal Name

RSCPublishing

ARTICLE

# Ultrafast Structural Dynamics in Rydberg Excited *N, N, N′, N′*-Tetramethylethylenediamine: Conformation Dependent Electron Lone Pair Interaction and Charge Delocalization

Type equation here. Cite this: DOI: 10.1039/xoxxoooooox

Received ooth January 2012,
Accepted ooth January 2012

DOI: 10.1039/xoxxoooooox

www.rsc.org/

Xinxin Cheng,[a] Yao Zhang,[a] Sanghamitra Deb,[b] Michael P. Minitti,[c] Yan Gao,[a] Hannes Jónsson[a,d] and Peter M. Weber*[a]

Two nitrogen atoms and a flexible carbon skeleton make *N, N, N', N'*-tetramethylethylenediamine (TMEDA) an important model system to study the interplay of conformeric motions and charge delocalization. Ionization of one of the nitrogen atoms generates a localized charge that may (partially) transfer to the other nitrogen. The structural motions, conformation dependent electron lone pair interaction and charge transfer in Rydberg-excited TMEDA, where the molecular ion core closely resembles the ion, were probed by time-resolved Rydberg fingerprint spectroscopy. Excitation to the 3p Rydberg level with a 209 nm laser pulse initially created a charge-localized ion core. Rapid internal conversion to the 3s Rydberg state yielded a multitude of conformational structures, in particular structures that are close to the folded $GG'G^+$ and $GGG'^+$ (see text for label definitions) core structures (235 fs), and structures that are close to the extended $TTT^+$ core structure (557 fs). The initial excitation and the internal conversion deposit about 1.89 eV of energy into the vibrational manifold, enabling a fast equilibrium between the folded and the extended structures. The forward and backward time constants were determined to be 490 fs and 621 fs, respectively. With the molecule highly vibrationally excited, the decay to 3s proceeds with a 6.77 ps time constant. Density functional theory (DFT) and *ab initio* calculations show evidence of strong lone pair interaction and charge delocalization in the equilibrium conformers. Importantly, DFT with self-interaction correction properly describes the binding energy of the Rydberg electron and provides excellent agreement with the experimental results.

## Introduction

Organic radical cations are important intermediates in biological and chemical systems that involve electron-transfer reactions.[1-7] With two ionization centers in one molecule, diamine systems including various lengths of carbon chains or rings between the two nitrogen atoms have been intensively studied as prototypes to explore electron lone pair interactions.[8-17] Two types of interactions, through-bond-interaction (TBI) and through-space-interaction (TSI) have been proposed theoretically[9] and observed experimentally.[8,11,12,16,17] Both types of interactions have been suggested to depend on the molecular structure. For example, a delayed onset of the charge-resonant electronic absorption signal of several aliphatic diamine radical cations in a rigid matrix environment was discovered in the early 1990's and interpreted as conformation-dependent intramolecular charge delocalization.[18,19] Recently, the charge transfer process linked to structural deformations of the molecular skeleton of *N,N'*-dimethylpiperazine (DMP) was monitored with ultrafast time resolution.[20] The structural dynamics of the DMP molecular cation towards a geometry that is favorable for lone pair interactions and charge delocalization was found to proceed with a time constant of several picoseconds.

In the present work we use time-resolved Rydberg fingerprint spectroscopy (RFS), density functional theory and *ab initio* calculations to study the conformation-dependent lone pair interaction and charge transfer in TMEDA, which has similar size but greater conformational flexibility than DMP. Like DMP, TMEDA appears to have negligible lone pair interactions in the ground state.[10-12,14] The situation in TMEDA therefore differs from that of diazabicyclo [2.2.2] octane (DABCO), which features well-known TBI in the ground electronic state.[8] This assessment of TMEDA is evidenced by its ionization potential and the electronic absorption spectrum, both of which are similar to those of tertiary monoamines of similar size.[11,21]

RFS takes advantage of the sensitivity of a Rydberg electron's binding energy (BE) to both the molecular structure of the ion core and the distribution of charges in the system.[22,23] Measurement of the Rydberg electron binding energy has been proven to be an effective tool to monitor molecular structural dynamics, including the conformational dynamics in hot flexible aliphatic molecules[24], the hydrogen transfer reaction in large van der Waals clusters[25], the charge transfer dynamics in bi-functional molecules[26] and in model molecules with two symmetry-equivalent ionization centers.[20] The dynamics in the Rydberg states should closely resemble that of the molecule in its ionic ground state because the effect of the Rydberg electron on the chemical bonds of the ion core is very small. Since the ejection of a photoelectron is fast compared to the motions of the ion core, the photoelectron spectra reflect the molecular structure at the time of electron ejection. Structural motions can be followed by introducing a time delay between the optical excitation of the Rydberg state and the ionization.[27]

## Experimental and theoretical method

The photoelectron spectroscopy and mass spectrometry apparatus has been described previously.[28,29] The photoelectrons and ions were detected using microchannel plate detectors. The flight times of the photoelectrons and ions were converted to kinetic energies and mass to charge ratios, respectively. The binding energy of an electron in a Rydberg state was determined by subtracting the kinetic energy from the probe photon energy. Femtosecond laser pulses were generated by a two-stage amplifier (a regenerative amplifier followed by a single pass amplifier, Coherent Legend Elite Duo) and an optical parametric amplifier (Coherent Opera SOLO). The regenerative amplifier, operating at 5 kHz repetition rate, produced fundamental pulses at 808 nm with about 35 fs duration. 90% of the fundamental was sent to the optical parametric amplifier (OPA) to generate the pump pulses at 209 nm, while 10% was upconverted using a BBO crystal to the second harmonic (404 nm) to be used as probe pulses. The time zero of the pump-probe pulse overlap was determined by monitoring the two-color mass signal from the OPA pulse excitation and second harmonic ionization of 1,4-dimethylpiperazine. The cross-correlation time between the pulses was measured to be 98(3) fs at FWHM. The energies of the pump and probe pulses were 0.3 μJ and 7.8 μJ, respectively. The laser beams were focused onto the molecular beam in the reaction region using a 500 mm concave mirror. The peak intensities at the focus of the pump and probe pulses were estimated as $7 \cdot 10^{10}$ W/cm$^2$ and $2 \cdot 10^{11}$ W/cm$^2$, respectively.

TMEDA was seeded in 1.1 bar of Helium carrier gas and expanded through a 100 μm nozzle followed by a 150 μm skimmer. To reduce the amount of clustering in the molecular beam, the liquid sample was cooled in a temperature-controlled bath at -20°C before entraining it in the stream of helium. TMEDA (ReagentPlus®, 99%) was purchased from Sigma-Aldrich and used without further purification.

Conformational local minima and global minimum searches in both the ground state and the ion state were performed using Gaussian 09.[30] Six C–N bonds and one C–C bond provide seven rotors in total, see Fig. 4 (a). However, only the rotations around the N1–C2 and N4–C3 bonds (shown in red) and the C2–C3 bond (shown in green) create new conformational structures. Each of the three rotors has three staggered positions, giving 27 initial configurations that were used as starting points for energy minimizations in a search for the most stable conformers. These conformers are labeled with "G", "T" and "G'", where G or *gauche*, T or *trans*, and G' or *gauche'* means that the dihedral angle D (LP–N–C–C) or D (N–C–C–N) is in the range of 0° to 120°, 120° to 240°, and 240° to 360° or -120° to 0°, respectively. LP stands for the electron lone pair of the N atom. These conformers were optimized at different levels of theory, including HF, MP2 and DFT with the PBE1PBE (also known as PBE0) functional with the Aug-cc-pVDZ basis set. Frequency calculations were performed to ensure the optimized structures were stable minima. The molecular orbitals were obtained at MP2/Aug-cc-pVDZ level of theory. The excitation energies and the binding energies of the Rydberg states of the optimized structures were calculated using density functional theory (DFT) with Perdew-Zunger self-interaction correction (SIC)[31], carried out with the GPAW program[32-34] in real space with a uniform grid. Briefly, the Rydberg orbitals were obtained using the ground state DFT-SIC with the local density approximation (LDA) functional. The total energy of the Rydberg excited state was obtained using the Delta Self-Consistent Field method[35] where one electron was removed from the highest occupied orbital (HOMO) and placed in the desired Rydberg orbital. The binding energy of the Rydberg excited state was then obtained by subtracting the total energy of the excited state energy from that of the ion. This approach to the calculation of Rydberg states has been described previously and shown to give good results.[36] The side length of the cubic simulation cell was 25 Å with a uniform grid size of 0.15 Å. The natural bond orbital (NBO) analysis[37] used to calculate the orbital interactions was conducted at the MP2/Aug-cc-pVDZ level using the Gaussian 09 built-in NBO Version 3.1 package.

## Results and discussion

The time-resolved two-color photoionization mass spectrum and the time-resolved photoelectron spectrum are shown in Fig. 1. The 209 nm (5.93 eV) pump pulse resonantly excites TMEDA to the 3p Rydberg state and the 404 nm (3.07 eV) probe pulse monitors the time-dependent dynamics by ionizing the Rydberg-excited molecules. The mass spectrum, Fig. 1 (a), shows a very short-lived parent peak at M/Z=116 and only a single fragment peak at M/Z=58. No signals of molecular clusters or from other fragment species were detected. Additionally, no cluster signal was found in the photoelectron spectrum at the binding energies typical for clusters[25]. We conclude that we indeed monitor the dynamics of TMEDA monomers in the collision-free environment of the molecular beam.

In analogy to our previous studies of other tertiary amines[38,39], we assign the short-lived peak with BE 2.15 eV to the 3p Rydberg state. The broad feature comprised of two peaks, at about 2.70 and 2.84 eV, arises from ionization out of the 3s Rydberg states. We label the component peaks 3s_l and 3s_h, where l and h denote the lower and higher BE, respectively. As shown in Fig. 1 (c), the time dependencies of the parent and the fragment mass peaks exactly mirror those of the 3p and 3s total signals, respectively. Independent fits of the two sets of time-dependent data give essentially the same time constants, as listed in Table 1. This implies that the ions generated by photoionization out of 3p don't fragment and rather remain intact on their path from the interaction region to



 

the mass spectrometer detector. In contrast, the synchronous time dependence of the fragment mass peak and the 3s Rydberg peak implies that the molecules ionized out of 3s end up as fragments. The photoionization out of a Rydberg state preserves the vibrational energy[38], and in the collision free molecular beam there is no transfer of energy to other molecules.

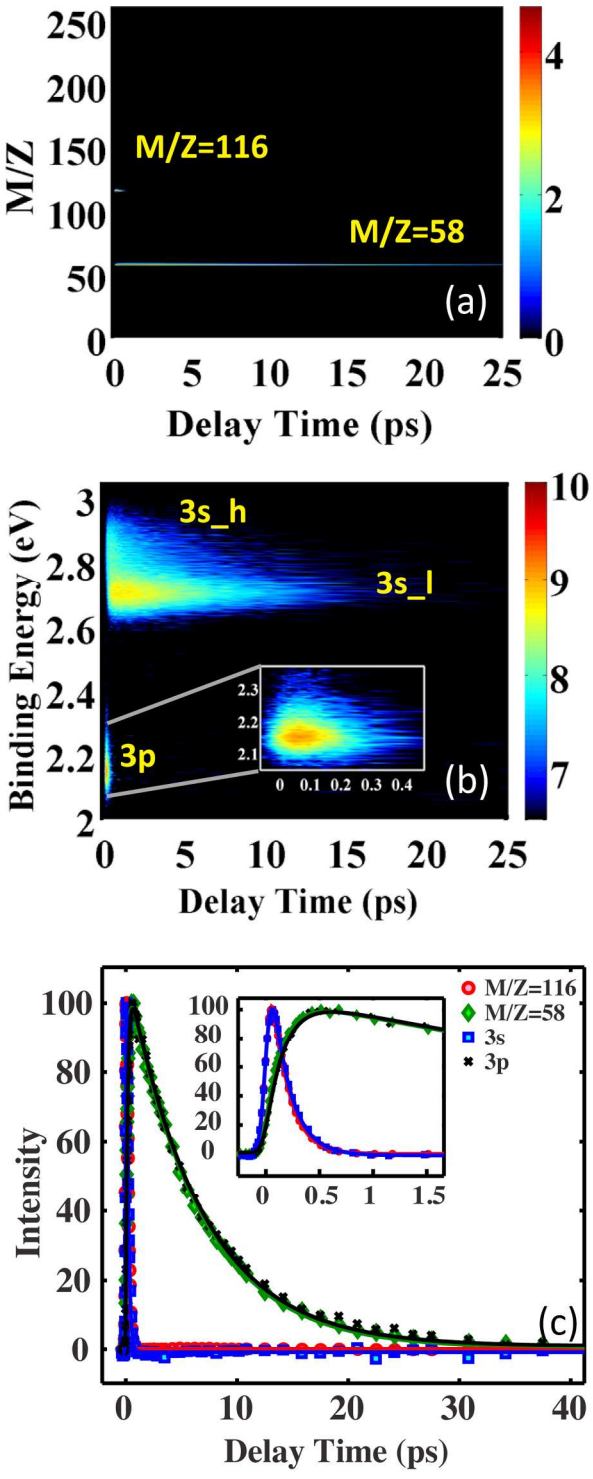


**Fig. 1** The time dependent spectra of TMEDA upon excitation with one photon at 209 nm and ionization at 404 nm. (a) The time dependent mass spectrum. (b) The time dependent Rydberg electron binding energy spectrum. The colors represent signal intensities on a logarithmic scale and the color bar gives the scale range in arbitrary units. 3s_h and 3s_l represent the two 3s component peaks with higher and lower BE, respectively. The inset spectrum shows the enlarged 3p peak during a smaller time window. (c) The time dependence of the total intensities of the parent peak (red circle), the only fragment peak (green diamond), the 3p peak (blue square) and the 3s peak (black cross). Solid lines represent the best fits of the experimental data using the Levenberg-Marquardt algorithm. The inset shows the enlarged peaks over a smaller time window. The main text of the article should go here with headings as appropriate.

**Table 1.** Time constants obtained in a global fit of time-dependent data of the mass and photoelectron spectra, together with uncertainties (3σ).

| Processes | Fit Parameters (3σ) |
|---|---|
| Decay of parent or rise of fragment | $t_1$=153 (5) fs |
| Decay of fragment | $t_2$=6.52 (0.17) ps |
| Decay of 3p or rise of 3s | $t_1$'=169 (7) fs |
| Decay of 3s | $t_2$'=6.59 (0.23) ps |

To explain these observations we note that optical excitation with 209 nm to the 3p level deposits about 1.34 eV of energy into vibrations. A detailed estimation of the vibrational energy is provided as supporting information. Apparently, this energy is not sufficient to dissociate a bond in the molecular ion. Consequently, ionization out of 3p generates ions that while highly vibrationally excited, are not sufficiently energetic to allow fragmentation. The internal conversion from 3p to 3s converts about 0.55 eV of electronic energy to vibrational energy. Ions generated by photoionization of the 3s state therefore have 1.89 eV of vibrational energy, which apparently does suffice to fragment the ion. Since only one fragment, at M/Z=58, was detected, the dissociation must occur only at the carbon-carbon bond.

The fragment mass signal and the 3s Rydberg signal decay to the baseline with a 6.6 ps time constant. Two reaction channels can account for this decay. The first mechanism invokes a dissociative σ* state of the ethylenic bridge crossing the 3s Rydberg surface. Electronic curve crossing produces neutral fragments, presumably in their ground electronic state, which are not ionized in the experiment. A similar σ*-crossing mechanism has been found in *N, N*-dimethylphenethylamine (PENNA), which also has two functional groups in one molecule.[26] The second mechanism available to TMEDA is a radiationless internal conversion to the ground electronic state. Because the molecule has a large amount of vibrational energy, the rate of the internal conversion is expected to be high. Previous work has shown that the lifetime of the 3s Rydberg state in *N, N*-dimethylisopropylamine (DMIPA) exponentially decreases with the amount of vibrational energy.[40] Both the curve crossing and the internal conversion will result in the observed decay of the 3s peak intensity.

Further insights into the molecular reaction dynamics are gleamed from the photoelectron spectrum, which shows two component peaks in the 3s region. To analyze the partially

overlapping component peaks, we fitted the spectra at each time delay point with two Lorentzians, resulting in binding average energies of 2.704 (0.008) eV and 2.841 (0.008) eV, respectively. Details of the fits and the time dependencies of the two 3s peak centers are given in the supporting information, Time-dependent original data and the best fit at each time point were assembled into a movie that is available as supporting information. The fits also provide population ratios, which were fitted as shown in Fig. 2 by adopting the formalism of a two-component equilibrium system that is suddenly displaced from its equilibrium.[41] This results in an equilibrium population ratio of 0.415 (0.027) and 0.585 (0.027) for the 3s_h and 3s_l peaks, respectively. The population ratio displacement was determined to be 0.269 (0.070) and the equilibrium time constant was obtained as 418 (189) fs. Also shown in Fig. 2 are the conformeric structures that we associate with the binding energies as discussed below.

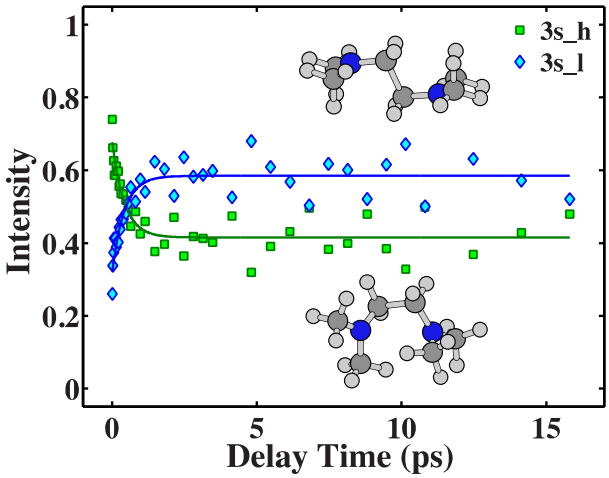


**Fig. 2** The time dependence of the component peaks representing the higher BE 3s peak (3s_h, green square, folded GGG'$^{+}$ structure at equilibrium) and the lower BE 3s peak (3s_l, blue diamond, extended TTT$^{+}$ structure at equilibrium).

The deconvoluted time dependencies of the individual 3s_h and 3s_l component intensities were obtained by multiplying the fit of the total 3s intensity by that of the 3s_h and 3s_l population ratios, respectively. Those data are represented as symbols in Fig. 3 (b). The normalized time-dependent intensities were then fitted using the kinetics model shown in Fig. 3 (a). The model assumes that there is only one ground state conformer present in the molecular beam and that it is excited directly to the 3p state by the 209 nm pump pulse. The 3p state decays to 3s states with higher (3s_h) and lower (3s_l) binding energies with time constants that are obtained as 235 fs and 557 fs, respectively. The internal conversion from 3p to 3s results in an initial, non-equilibrium population distribution of 3s_h (68.4%) and 3s_l (31.6%) states. Both the movie in the supporting information and the time-dependent population ratio in Fig. 2 show that after the initial internal conversion from 3p, the relative 3s_h population decreases while the 3s_l population increases. The 3s_l peak dominates at long delay times. Assuming first order kinetics, the model of Fig. 3 (a) allows for an equilibrium between 3s_h and 3s_l states that is approached with time constants of 490 fs and 621 fs for the forward and backward reactions, respectively. All the kinetics parameters obtained from the fit are listed in Table 2. In this model, both 3s peaks decay to the baseline with a time constant of 6.77 ps, which is within the 3σ error of the fits in Table 1. Because the time constants (490 fs and 621 fs) for the forward and backward reactions are comparable with the time constants of the internal conversion (235 fs and 557 fs), there are no visually obvious separations of the two rise times in the 3s_l peak intensity of Fig. 3 (b). In the 3s_h peak intensity, however, because of the very different time constants for the equilibrium and the slow decay to baseline, one can clearly discern the double exponential decay that results from the kinetics of the system (see the inset in Fig. 3 (b)).

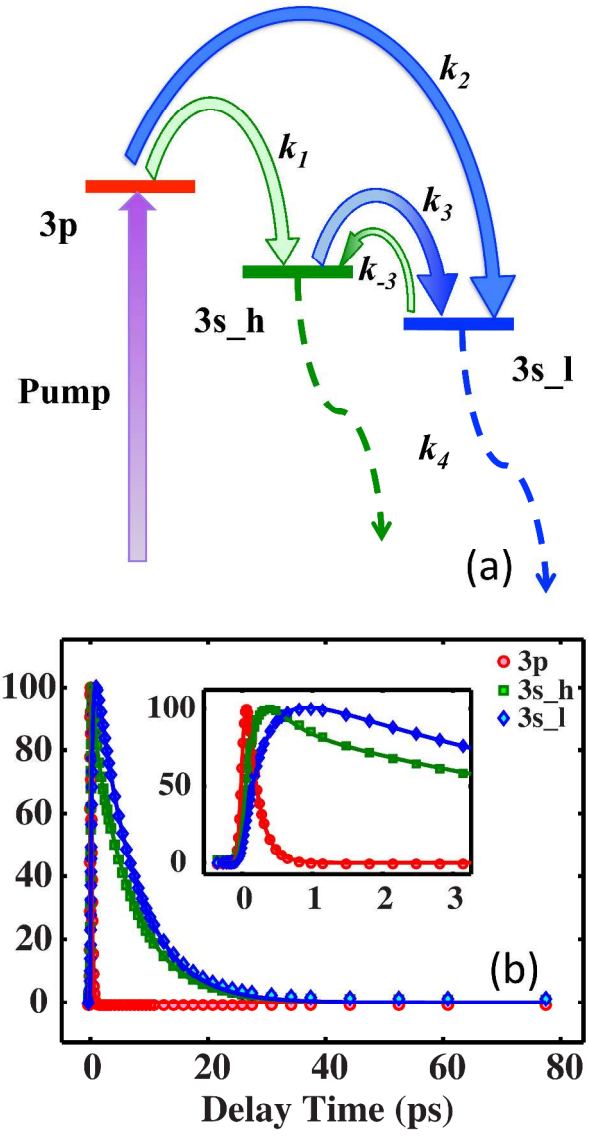


**Fig. 3** (a) The kinetics scheme used to obtain the best fit of the experimental data, assuming first order kinetics for all processes. The purple arrow shows the direct excitation to the 3p state. Solid green and blue arrows represent a transition to the 3s_h and 3s_l state, respectively. The dashed arrows show the decay of the 3s states. (b) The time-dependent signals of three distinct spectral features (3p in red circle, 3s_h in green

squares and 3s_l in blue diamonds). Solid lines represent the best fits of the experimental data using the Levenberg-Marquardt algorithm with the kinetics model shown in panel (a). The values of all the fit parameters are listed in Table 2.

**Table 2.** Time constants obtained in a global fit of all time-dependent data, together with uncertainties (3σ).

| Processes | Fit Parameters (3σ) |
|---|---|
| Internal conversion: decay from 3p to 3s_h | $\tau_1$=235 (16) fs |
| Internal conversion: decay from 3p to 3s_l | $\tau_2$=557 (45) fs |
| Equilibrium: 3s_h to 3s_l | $\tau_3$=490 (55) fs |
| Equilibrium: 3s_l to 3s_h | $\tau_{-3}$=621 (56) fs |
| Slow decay of 3s | $\tau_4$=6.77 (0.11) ps |

We draw attention to the asymmetric shape of the 3p peak as seen in the inset of Fig. 1 (b). The asymmetry could come about in two ways. First, it might result from the different magnetic quantum number components of the 3p level. This is the assumption inherent in the analysis we have presented above. Alternatively, one might propose that the asymmetry arises from the presence of two ground state conformers in the molecular beam. Each such conformer might give rise to a slightly different binding energy peak. In that picture, the two 3s peaks might then result from the internal conversion of the 3p states of the two conformers. Analyzing the data using that model we find, however, that it does not yield a self-consistent analysis. The decay times for the 3p peak at different binding energies, slightly above and below of the peak maximum, are almost identical (not shown here). The time constants for the rises of the two 3s peaks, however, are very different. If the two conformers were responsible for the 3p and 3s peak splittings, the decay and rise time constants should match each other. But that is not what we find in TMEDA's time-dependent data. Therefore, we conclude that our data show evidence for only one conformer present in the beam.

Calculations of the molecular and the cation ground states were carried out with the objective to assign conformeric structures of TMEDA to the observed spectrum. We assume that the effect of the Rydberg electron on the structure of the molecular ion core is negligible. Seven stable conformer categories in the ground state were found by rotating the two N–C bonds (N1–C2 and N4–C3) and the C2–C3 bond highlighted in Fig. 4 (a) by red and green colors, respectively. Structures obtained by minimizing the energy obtained from MP2/Aug-cc-pVDZ are shown in Fig. 4 (b) – (h). The full coordinates of the optimized structures in the ground state are provided in Table S1 in the supporting information. The relative energies calculated at different levels of theory are listed in Table 3. Conformers listed in parentheses are the same as or enantiomers of the conformer outside of the parentheses and are therefore grouped in the same category. According to the calculation, the global minimum in the ground state is the folded GG'G conformer shown in Fig. 4 (f). This is in good agreement with other theoretical studies of the TMEDA conformers in the ground state.[42,43] The computational results suggest that the folded GG'G TMEDA should be the conformer present in the cold molecular beam, implying that the molecules are cooled well by the supersonic expansion. A similar conclusion was drawn in our recent study of the structural dynamics of triethylamine (TEA)[44] where only one TEA ground state conformer is present in the molecular beam. In contrast, our experiments on *N, N*-dimethyl-2-butanamine (DM2BA) and *N, N*-dimethyl-3-hexanamine (DM3HA) showed that in these systems, the room temperature distribution of conformers is frozen in the molecular beam.[24] To understand these peculiarities, further studies of collision induced barrier crossings would be called for.

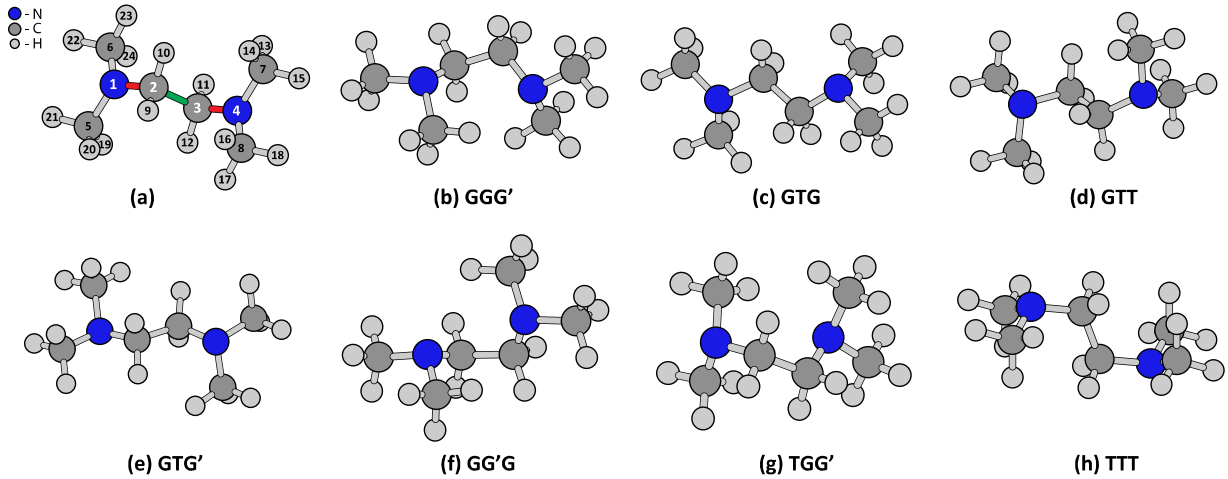


**Fig. 4** (a) Example TMEDA structure with atom numbers. The N1–C2 and N4–C3 bonds (red) and C2–C3 bond (green) show the three rotors that can generate new conformers. (b) – (h) Stable TMEDA conformers in the ground state. Each conformer is labeled with G, T and G' according to the nomenclature described in the text.

For the ion, five stable $TMEDA^+$ conformers were found by optimizing the structures on the ion potential surface starting with the stable ground state structures. The optimized structures are shown in Fig. 5. The full coordinates of the optimized structures in the ion ground state are given in Table S2 in the supporting information. Starting the optimization with the ground state global minimum GG'G conformer on the ion potential surface gave the $GG'G^+$ structure shown in Fig. 5 (c). The $TTT^+$ conformer with the extended structure shown in Fig. 5 (e) was found to be the global minimum in the ion ground state. The charge localized $GG'T^+$ structure, which is the same as $TGG'^+$ shown in Fig. 5 (d), was obtained for comparison by

optimizing the GG'G conformer with N4 semi-planar as a starting structure on the ion potential surface. The relative energies calculated by MP2/Aug-cc-pVDZ are listed in Table 3.

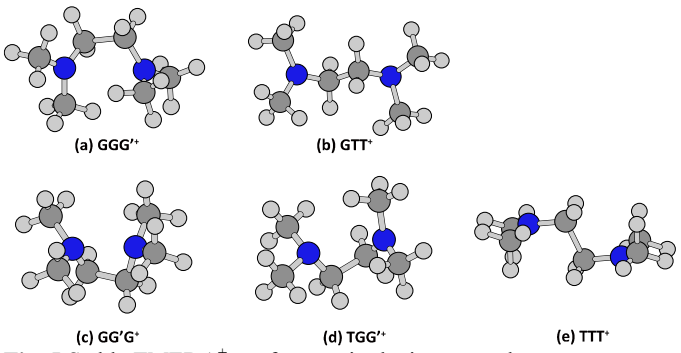


**Fig. 5** Stable $TMEDA^+$ conformers in the ion ground state.

**Table 3.** Relative energies[a] of conformers of TMEDA at different levels of theory with the Aug-cc-pVDZ basis set, and conformers of $TMEDA^+$ calculated by MP2/Aug-cc-pVDZ.

| | TMEDA | | | $TMEDA^+$ |
|---|---|---|---|---|
| Conformers | HF | PBE1PBE | MP2 | MP2 |
| GGG' (G'GG, G'G'G, GG'G') | 48 | 17 | 31 | 136 |
| GTG (G'TG') | 1 | 8 | 35[b] | 0[c] |
| GTT (TTG, G'TT, TTG') | 58 | 65 | 106 | 693 |
| GTG' (G'TG) | 0 | 11 | 47 | 693[c] |
| GG'G (G'GG') | 25 | 0 | 0 | 231 |
| TGG' (G'GT, TG'G, GG'T) | 91 | 64 | 66[b] | 458 |
| TTT | 127 | 140 | 194[b] | 0 |

[a] Values are in the unit of meV.
[b] The GGG (G'G'G') conformer, the GGT (TGG, G'G'T, TG'G') conformer and the TGT (TG'T) conformer changed to GTG (G'TG'), TGG' (G'GT, TG'G, GG'T) and TTT conformers, respectively, in the ground state optimization.
[c] The GTG (G'TG') conformer and the GTG' (G'TG) conformer changed to the TTT conformer and the G'TT conformer, respectively, in the ion optimization.

Binding energies of the 3s Rydberg state were calculated with the structures of the three most stable ion conformers, $TTT^+$, $GGG'^+$ and $GG'G^+$, assuming a negligible effect of the Rydberg electron on the structure of the molecular ion core. The calculated relative energies and binding energies are listed in Table 4. The calculated binding energies of 3s states with the $GGG'^+$ and $TTT^+$ structures, 2.848 eV and 2.706 eV respectively, are in excellent agreement with the experimental peak centers of the 3s_h and 3s_l components, 2.841 (0.008) eV and 2.704 (0.008) eV, respectively. In the experiment, 1.89 eV of energy is deposited into vibrational modes. Using the computed vibrational frequencies of the ion and assuming that the energy is equipartitioned among all the vibrational modes[37], the temperature of the molecule in the 3s Rydberg state can be estimated as 915 K. The energy difference between the 3s states with $GGG'^+$ and $TTT^+$ structures, 0.045 eV, therefore, will lead to a population ratio of 36.1% and 63.9% for 3s states with $GGG'^+$ and $TTT^+$ molecular ion cores, respectively, assuming a Boltzmann distribution at the equilibrium. However, the 3s_h peak is quite broad, indicating that more than one structure contributes to this peak component.[38] Taking both $GG'G^+$ and $GGG'^+$ into account for the higher binding energy 3s peak, the population ratio is expected to be 37.7% and 62.3% for the higher and lower binding energy 3s peaks, respectively. This matches quite well the experimental observation, which is 41.5% and 58.5% for the 3s_h and 3s_l populations, respectively, at equilibrium. We conclude that the major features of the 3s peaks at equilibrium arise from the 3s states with $GGG'^+$ and $TTT^+$ molecular ion cores, as shown in Fig. 2. $GG'G^+$ has a small contribution to the high binding energy signal.

**Table 4.** Calculated (using self-interaction corrected DFT) relative energies (RE) and binding energies (BE) of the 3s Rydberg state of TMEDA with the three most stable ion structures.

| Structures | RE/eV | BE/eV |
|---|---|---|
| $GG'G^+$ | 0.254 | 2.884 |
| $GGG'^+$ | 0.045 | 2.848 |
| $TTT^+$ | 0.000 | 2.706 |

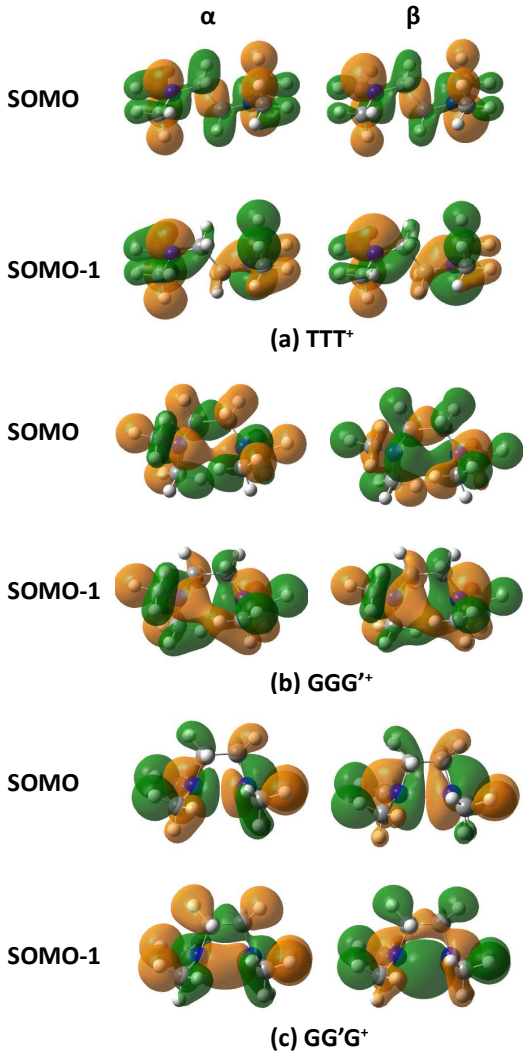


**Fig. 6** SOMO and SOMO-1 of the TMEDA cations with equilibrium structures: (a) $TTT^+$ (b) $GGG'^+$ and (c) $GG'G^+$. α

and β are used to label the spin. The α spin orbital of SOMO contains the unpaired electron.

As Fig. 6 (c) shows, the electron lone pairs of the TMEDA cation in the folded GG'G$^+$ structure are very close and may overlap effectively. As proposed previously[9], lone pair electrons in close spatial proximity can have TSI, which lowers the energy of the cation. The GG'G$^+$ structure has a geometry that is suitable for such interaction. A similar effect has been seen in the protonated TMEDA, TMEDAH$^+$, where the folded $G^{\mp}G^{\pm}G^{\mp}$ structure is the global minimum because of the strong intramolecular 1,4-N–H$^+$···N hydrogen bonding.[45] The energy ordering of the singly occupied molecular orbital (SOMO) and SOMO-1 of GG'G$^+$, which shows an antisymmetric and an symmetric combination of the two lone pairs in the SOMO and SOMO-1, respectively, is in agreement with the predicted consequence of the TSI.[9] The lone pairs of the extended TTT$^+$ and folded GGG'$^+$ structures shown in Fig. 6 (a) and (b) respectively, however, assume a geometry that is suited for TBI[9]. The lone pairs are well aligned and coupled with the C2–C3 σ bond, as is required for TBI. The energy ordering of the SOMO and SOMO-1 of TTT$^+$ and GGG'$^+$ shows a symmetric and antisymmetric combination of the two lone pairs in the SOMO and SOMO-1, respectively. This also matches the predicted consequence of the TBI.[9] The fact that both the extended TTT$^+$ and folded GGG'$^+$ structures have significant TBI shows an insensitivity of the TBI coupling to the rotation around the C2–C3 σ bond since it will not change the coupling overlap.[9] The stability gain resulting from TBI must be larger than that of TSI in the TMEDA$^+$ molecule, since overall the GGG'$^+$ and TTT$^+$ conformers have much lower energies. In the TMEDAH$^+$ molecule, where only one lone pair exists, the hydrogen bonding dominates.

**Table 5.** Selected bond lengths, dihedral angles optimized by MP2/Aug-cc-pVDZ and NBO analysis of the ground state and ion structures at the same level of theory: natural charges on the nitrogen atoms, Wiberg bond indices of N1···N4 and C2–C3, occupancies in the bonding and antibonding NBOs of N1···N4, C2–C3 and the lone pairs, and the second-order perturbation energies $E(2)$ (donor → acceptor) involving the bonding and antibonding NBOs of N1···N4, C2–C3 and the lone pairs.

| | GG'G | GG'T$^+$ | GG'G$^+$ | GGG'$^+$ | TTT$^+$ |
|---|---|---|---|---|---|
| B(C2, C3) [a] | 1.532 | 1.551 | 1.531 | 1.623 | 1.634 |
| D(N1, C2, C3, N4) [a] | -45.040 | -51.355 | -30.987 | 57.972 | -180.000 |
| NC(N1) [b] | -0.647 | -0.678 | -0.386 | -0.426 | -0.400 |
| NC(C2) | -0.161 | -0.166 | -0.172 | -0.157 | -0.158 |
| NC(C3) | -0.161 | -0.210 | -0.172 | -0.157 | -0.158 |
| NC(N4) | -0.647 | -0.031 | -0.387 | -0.426 | -0.400 |
| WBI(N1, N4) [c] | 0.007 | 0.005 | 0.200 | 0.101 | 0.091 |
| WBI(C2, C3) | 1.010 | 0.982 | 1.007 | 0.837 | 0.794 |
| BD(C2, C3) [d] | 1.98326 | 0.99257(α), 0.97278(β) | 0.99175(α), 0.99152(β) | 0.99195(α), 0.87672(β) | 0.99348(α), 0.85053(β) |
| BD*(C2, C3) [d] | 0.01428 | 0.01039(α), 0.00732(β) | 0.00815(α), 0.00180(β) | 0.01812(α), 0.05409(β) | 0.02125(α), 0.07097(β) |
| BD(N1, N4) | | | 0.94952(β) | 0.24707(β) | 0.26000(β) |
| BD*(N1, N4) | | | 0.07476(β) | 0.89193(β) | 0.87394(β) |
| LP(N1) [d] | 1.91083 | 0.9598(α), 0.95969(β) | 0.97246(α) | 0.96251(α) | 0.96297(α) |
| LP(N4) | 1.91085 | 0.97178(α) | 0.97245(α) | 0.96251(α) | 0.96297(α) |
| BD(C2, C3) --> BD(N1, N4) [e] | | | | 34.06(β) | 39.40(β) |
| BD(C2, C3) --> LP*(N4) | | 7.90(β) | | | |
| BD(C7, H15) --> LP*(N4) | | 11.08(β) | | | |
| BD(C8, H17) --> LP*(N4) | | 12.86(β) | | | |
| LP(N1) --> BD*(C2, C3) | | | | 5.64(α) | 6.44(α) |
| LP(N1) --> BD*(C2, H10) | 11.28 | 5.35(α), 5.23(β) | | | |
| LP(N1) --> BD*(C5, H21) | 10.76 | | | | |
| LP(N1) --> BD*(C6, H22) | 10.38 | | | | |
| LP(N4) --> BD*(C2, C3) | | | | 5.64(α) | 6.44(α) |
| LP(N4) --> BD*(C3, H11) | 11.28 | | | | |
| LP(N4) --> BD*(C7, H14) | 10.37 | | | | |
| LP(N4) --> BD*(C8, H16) | 10.76 | | | | |
| BD*(N1, N4) --> BD*(C2, C3) | | | | 27.35(β) | 33.18(β) |
| BD(C8, H16) --> BD*(N1, N4) | | | 5.54(β) | | |

[a] Bond lengths in Å, dihedral angles in deg.
[b] NC means the natural charges from the NBO analysis.
[c] WBI is short for Wiberg bond index, indicating the bond order.
[d] BD, BD* and LP give the types of bonding, antibonding and lone pair NBOs, respectively.

[e] Energies in kcal/mol. α, β in parenthesis means α or β spin orbitals. The α spin orbital of SOMO contains the unpaired electron. Only values larger than 10 kcal/mol in the ground state or larger than 5 kcal/mol in the ion are listed in the table.

The above analysis is supported by NBO calculations, which show evidence of the interactions and charge delocalization in the equilibrium structures (see Table 5). In the ground state GG'G, the lone pairs interact independently with the C–H bonds with which they are aligned well. In the charge-localized ion GG'$T^+$, the lone pairs also behave independently. However, in the charge-delocalized ions GGG'$^{+}$ and $TTT^+$, the lone pairs from N1 and N4 form bonding and antibonding NBOs that have significant interaction with the C2–C3 bond. This interaction results in a large increase of the $\sigma^*_{C2-C3}$ occupancy in the ions, compared to that in the ground states GG'G and the charge-localized ion GG'$T^+$. It is consistent with the smaller Wiberg bond indices and longer bond lengths seen in GGG'$^{+}$ and $TTT^+$. Table 5 also shows a significant increase in the occupancies of the N1···N4 bonding and antibonding NBOs and the values of the Wiberg bond indices, indicating strong TBI interaction between the two lone pairs. The interaction may lead to a (partial) charge transfer from one nitrogen atom to the other. Natural charge analysis shows a complete charge delocalization in GGG'$^{+}$ and $TTT^+$, where both nitrogen atoms are equivalent and have the same charge.

The GG'$G^+$ conformer has a significant occupancy and a large Wiberg bond index of the N1···N4 bond and a delocalized natural charge on the two nitrogen atoms. Its C2–C3 bond length, Wiberg bond index and the $\sigma^*_{C2-C3}$ occupancy are all very close to those of the ground state GG'G and the charge-localized ion GG'$T^+$. Combined, these observations suggest TSI in the GG'$G^+$ conformer.

Summarizing these calculations, the structural dynamics, the conformation dependent lone pair interaction and the charge delocalization in Rydberg-excited TMEDA molecules can be described as follows. The excitation of the ground state molecules to the 3p Rydberg state preserves, at time zero, the initial GG'G structure. Since the interaction of the nitrogen lone pair electrons is negligible in the ground state, only one of the lone pair electrons is excited to the Rydberg orbital, leaving the charge localized at one nitrogen atom. The experiments show that rapid internal conversion from 3p to 3s simultaneously populates the folded and extended conformers with a non-equilibrium ratio. The time span of the optical excitation and the relaxation to 3s is short: the time constants are 235 fs and 557 fs for the internal conversion from the 3p Rydberg state with a molecular ion core in the Franck-Condon structure to the 3s Rydberg states with the folded cores and the extended cores, respectively. Consequently, the most suitable geometries for all the internal rotational degrees of freedom and lone pair interactions are not immediately found. Right after the internal conversion, the initial population ratios of the folded and extended structures are also at non-equilibrium values. Once the system leaves the Franck-Condon region it can sample the multi-dimensional potential energy surface until it finds the most stable structures where the electron lone pairs have strong interactions and the charge can delocalize. Two types of lone pair interactions, TBI and TSI are found in the equilibrium ion structures and are responsible for the charge delocalization. The large amount of internal vibrational energy (1.89 eV), which corresponds to a vibrational temperature of 915 K, enables the molecule to clear the barriers, leading to an equilibrium between the structures GGG'$^{+}$ and GG'$G^+$ and the structure $TTT^+$, with forward and backward time constants of 490 fs and 621 fs.

## Conclusion and perspectives

The ultrafast structural dynamics, conformation dependent lone pair interaction and charge delocalization in Rydberg excited TMEDA molecules were explored using time-resolved RFS coupled with computer simulations. Excitation with 209 nm pump pulses places the molecule in a charge-localized 3p state of the folded GG'G structure. Rapid internal conversion from 3p to 3s populates both folded and extended structures at non-equilibrium geometries and in a non-equilibrium population ratio. As in the previously studied DMP molecule, the internal conversion leads to a mixture of specific conformeric forms rather than to a uniform spreading over the entire available phase space. This implies that the internal conversion is non-ergodic, supporting a suggestion that has recently been derived from the study of other molecules based on the observation of the levels from which the internal conversion originates.[46] A full understanding of the structural aspects of the internal conversion in diamines remains elusive.

Once the internal conversion is complete, the molecules very quickly sample the potential energy surface and approach an equilibrium distribution of local minima representing mostly the GGG'$^{+}$ and $TTT^+$ conformeric structures. The time constants for the forward and backward reactions of the equilibrium were significantly faster than those of the related, but structurally more rigid DMP molecule that was previously investigated.[20] This can be rationalized by the lower rigidity of the molecular skeleton in TMEDA.

The equilibrium structures show evidence for lone pair interactions and charge delocalization. Because the motions of the electrons are too fast to monitor, the pump-probe experiment does not directly observe how the electron transfers in the molecule. But the binding energy spectrum does reveal, in real time, how the geometrical structure of the Rydberg-excited molecule changes from the one initially excited to one where the charge is fully delocalized.

RFS remains the experimental tool of choice to probe the structural dynamics of molecular systems in the presence of large amounts of vibrational energy, which is often needed to explore chemical reactions. The large size of the Rydberg orbital and the sensitivity of the Rydberg electron's binding energy on the molecular structure make RFS a potent tool to observe the conformation dependent interactions and charge transfer reactions in large molecules. The present exploration of TMEDA serves as a model to demonstrate the ability of RFS to monitor the conformation dependent processes in real time. The ability of the DFT-SIC calculations with GPAW to accurately calculate the binding energies is extremely advantageous to positively identify the molecular structures from the observed spectra.

Further experiments with varying pump wavelengths could be used to determine experimentally the energy difference between the 3s Rydberg states with the molecular ion core structures GGG'$^{+}$ and $TTT^+$. Electron or x-ray diffraction at similar molecular beam conditions would be beneficial to



 

confirm independently the molecular structures and conformational distributions.

## Acknowledgements
This project was supported, in part, by the Division of Chemical Sciences, Geosciences, and Biosciences, the Office of Basic Energy Sciences, the U.S. Department of Energy by Grant No. DE-FG02-03ER15452. The simulation and energy calculations of the molecular structures were conducted using computational resources and services at the Center for Computation and Visualization, Brown University.

## Key words
Conformational Dynamics; Lone Pair Interaction; Charge Transfer; Excited States; Photoelectron Spectroscopy.

## Notes and references
[a] Department of Chemistry, Brown University, Providence, RI 02912, United States.
[b] Department of Chemistry, Duke University, Durham, NC 27708, United States.
[c] Linac Coherent Light Source (LCLS), SLAC National Accelerator Laboratory, Menlo Park, CA 94025, United States.
[d] Faculty of Physical Sciences, VR-III, University of Iceland, 107 Reykjavík, Iceland.
[*] To whom correspondence should be addressed. Tel.: +1-401-8633767; fax: +1-401-8632594. E-mail: peter_weber@brown.edu.

† Electronic Supplementary Information (ESI) available: The movie showing the Lorentzian fits of the overlapped 3s peaks at each time point; analysis of the binding energy spectrum; vibrational energy content of TMEDA in the 3p and 3s Rydberg states; structures of TMEDA and $TMEDA^+$ conformers. See DOI: 10.1039/b000000x/

1 L. Sanii and G. B. Schuster, *J. Am. Chem. Soc.*, 2000, **122**, 11545-11546.
2 M. Schmittel and A. Burghart, *Angew. Chem. Int. Edit.*, 1997, **36**, 2550-2589.
3 A. A. Voityuk, *J. Phys. Chem. B*, 2005, **109**, 10793-10796.
4 A. H. Zewail, *J. Phys. Chem. A*, 2000, **104**, 5660-5694.
5 E. R. Gaillard and D. G. Whitten, *Acc. Chem. Res.*, 1996, **29**, 292-297.
6 H. D. Roth, *Acc. Chem. Res.*, 1987, **20**, 343-350.
7 S. Gronert, *Chem. Rev.*, 2001, **101**, 329-360.
8 E. Heilbronner and K. A. Muszkat, *J. Am. Chem. Soc.*, 1970, **2**, 3818-3821.
9 R. Hoffmann, *Acc. Chem. Res.*, 1971, **4**, 1-9.
10 S. F. Nelsen and J. M. Buschek, *J. Am. Chem. Soc.*, 1974, **96**, 7930-7934.
11 A. M. Halpern and T. Gartman, *J. Am. Chem. Soc.*, 1974, **96**, 1393-1398.
12 A. M. Halpern, B. R. Ramachandran and S. Sharma, *J. Phys. Chem.*, 1982, **86**, 2049-2052.
13 R. W. Alder, R. J. Arrowsmith, A. Casson, R. B. Sessions, E. Heilbronner, B. Kovac, H. Huber and M. Taagepera, *J. Am. Chem. Soc.*, 1981, **103**, 6137-6142.
14 M. Braga and S. Larsson, *J. Phys. Chem.*, 1992, **96**, 9218-9224.
15 C. X. Liang and M. D. Newton, *J. Phys. Chem.*, 1992, **96**, 2855-2866.
16 A. M. Brouwer, F. W. Langkilde, K. Bajdor and R. Wilbrandt, *Chem. Phys. Lett.*, 1994, **225**, 386-390.
17 A. M. Brouwer, J. M. Zwier, C. Svendsen, O. S. Mortensen, F. W. Langkilde and R. Wilbrandt, *J. Am. Chem. Soc.*, 1998, **120**, 3748-3757.
18 A. Marcinek, J. Gebicki and A. Plonka, *J. Phys. Org. Chem.*, 1990, **3**, 757-759.
19 J. Gebicki, A. Marcinek and C. Stradowski, *J. Phys. Org. Chem.*, 1990, **3**, 606-610.
20 S. Deb, X. X. Cheng and P. M. Weber, *J. Phys. Chem. Lett.*, 2013, **4**, 2780-2784.
21 A. M. Halpern, J. L. Roebber and K. Weiss, *J. Chem. Phys.*, 1968, **49**, 1348-1357.
22 J. L. Gosselin and P. M. Weber, *J. Phys. Chem. A*, 2005, **109**, 4899-4904.
23 N. Kuthirummal and P. M. Weber, *Chem. Phys. Lett.*, 2003, **378**, 647-653.
24 M. P. Minitti and P. M. Weber, *Phys. Rev. Lett.*, 2007, **98**, 253004.
25 S. Deb, M. P. Minitti and P. M. Weber, *J. Chem. Phys.*, 2011, **135**, 044319.
26 J. C. Bush, M. P. Minitti and P. M. Weber, *J. Phys. Chem. A*, 2010, **114**, 11078-11084.
27 A. Stolow, *Annu. Rev. Phys. Chem.*, 2003, **54**, 89-119.
28 B. J. Kim, N. Thantu and P. M. Weber, *J. Chem. Phys.*, 1992, **97**, 5384-5391.
29 W. Cheng, N. Kuthirummal, J. L. Gosselin, T. I. Solling, R. Weinkauf and P. M. Weber, *J. Phys. Chem. A*, 2005, **109**, 1920-1925.
30 Gaussian 09, Revision **C.01**, M.J. Frisch, G.W. Trucks, H.B. Schlegel, G.E. Scuseria, M.A. Robb, J.R. Cheeseman, G. Scalmani, V. Barone, B. Mennucci, G.A. Petersson et al. Gaussian, Inc., Wallingford CT, 2009.
31 J. P. Perdew and A. Zunger, *Phys. Rev. B*, 1981, **23**, 5048-5079.
32 J. J. Mortensen, L. B. Hansen and K. W. Jacobsen, *Phys. Rev. B*, 2005, **71**, 035109.
33 J. Enkovaara, C. Rostgaard, J. J. Mortensen, J. Chen, M. Dulak, L. Ferrighi, J. Gavnholt, C. Glinsvad, V. Haikola, H. A. Hansen, et al., *J. Phys.: Condens. Matter*, 2010, **22**, 253202.
34 A. Valdes, J. Brillet, M. Gratzel, H. Gudmundsdottir, H. A. Hansen, H. Jonsson, P. Klupfel, G. J. Kroes, F. Le Formal, I. C. Man, et al., *Phys. Chem. Chem. Phys.*, 2012, **14**, 49-70.
35 J. Gavnholt, T. Olsen, M. Engelund and J. Schiotz, *Phys. Rev. B*, 2008, **78**, 075441.
36 H. Gudmundsdottir, Y. Zhang, P. M. Weber and H. Jonsson, *J. Chem. Phys.*, 2013, **139**, 194102.
37 NBO Version 3.1, E. D. Glendening, A. E. Reed, J. E. Carpenter, and F. Weinhold.
38 M. P. Minitti, J. D. Cardoza and P. M. Weber, *J. Phys. Chem. A*, 2006, **110**, 10212-10218.
39 J. L. Gosselin, M. P. Minitti, F. M. Rudakov, T. I. Solling and P. M. Weber, *J. Phys. Chem. A*, 2006, **110**, 4251-4255.
40 F. Rudakov, Y. Zhang, X. Cheng and P. M. Weber, *Opt. Lett.*, 2013, **38**, 4445-4448.
41 P. L. Houston, *Chemical Kinetics and Reaction Dynamics*, McGraw-Hill, New York, 2001.

42 D. Y. Wu, Y. Ren, X. Wang, A. M. Tian, N. B. Wong and W.-K. Li, *J. Mol. Struct. Theochem*, 1999, **459**, 171-176.
43 N. B. Wong, Y. S. Cheung, D. Y. Wu, Y. Ren, A. M. Tian and W. K. Li, *J. Phys. Chem. A*, 2000, **104**, 6077-6082.
44 S. Deb, B. A. Bayes, M. P. Minitti and P. M. Weber, *J. Phys. Chem. A*, 2011, **115**, 1804-1809.
45 K. Ohno, T. Kuriyama, M. Fukuda, H. Yoshida and H. Matsuura, *Chem. Lett.*, 2000, **12**, 1406-1407.
46 T. S. Kuhlman, T. I. Solling and K. B. Moller, *ChemPhysChem*, 2012, **13**, 820-827.